Published online 3 July 2008

Nucleic Acids Research, 2008, Vol. 36, No. 13 ***4433–4442***
doi:10.1093/nar/gkn402

Effect of loop length variation on quadruplex-Watson Crick duplex competition

Niti Kumar[1], Bankanidhi Sahoo[2], K. A. S. Varun[2], Sudipta Maiti[2] and Souvik Maiti[1,*]

[1]Proteomics and Structural Biology Unit, Institute of Genomics and Integrative Biology, CSIR, Mall Road, Delhi 110 007 and [2]Department of Chemical Sciences, Tata Institute of Fundamental Research, Homi Bhabha Road, Colaba, Mumbai 400005, India

Received February 4, 2008; Revised June 7, 2008; Accepted June 9, 2008

ABSTRACT

The effect of loop length on quadruplex stability has been studied when the G-rich strand is present along with its complementary C-rich strand, thereby resulting in competition between quadruplex and duplex structures. Using model sequences with loop lengths varying from T to T5, we carried out extensive FRET to discover the influence of loop length on the quadruplex-Watson Crick duplex competition. The binding data show an increase in the binding affinity of quadruplexes towards their complementary strands upon increasing the loop length. Our kinetic data reveal that unfolding of the quadruplex in presence of a complementary strand involves a contribution from a predominant slow and a small population of fast opening conformer. The contribution from the fast opening conformer increases upon increasing the loop length leading to faster duplex formation. FCS data show an increase in the interconversion between the quadruplex conformers in presence of the complementary strand, which shifts the equilibrium towards the fast opening conformer with an increase in loop length. The relative free-energy difference ($\Delta\Delta G^{\circ}$) between the duplex and quadruplex indicates that an increase in loop length favors duplex formation and out competes the quadruplex.

INTRODUCTION

The fundamental unit of the G-quadruplex (1,2) is a square planar arrangement of guanines, where each guanine accepts and donates two Hoogsteen hydrogen bonds, placing four electronegative carbonyl groups towards the interior of the tetrad. These quartets are then stabilized by monovalent cations (3), which form cation-dipole interactions with the eight guanines, reduce the repulsion of central oxygen atoms, enhance hydrogen bond strength and stabilize quartet stacking. Interest in these structures has increased markedly in the past decade, as the evidence for their possible functional roles *in vivo* has accumulated. These guanine-rich segments are found in biologically significant regions of the genome such as telomeres (4), immunoglobulin switch regions (5) and promoter regions of eukaryotic cells (6–8). The interconversion between double- or single-stranded DNA and G-quadruplex in cells is dependent upon a number of cellular proteins (9). Some of these proteins include the β-subunit of the *Oxytricha* telomere-binding protein (10), *Saccharomyces cerevisiae* Rap1 (11), Sgs1 (12), Hop1 (13), Mre11 (14), Kem1 (15) proteins and human nuclease with G4 selectivity (16). A number of proteins interacting specifically with G-quadruplexes have been implicated in diseases like Bloom's (17) and Werner's syndromes (18).

Recent bioinformatics studies have found that sequences which can fold into G- quadruplex structures are widely dispersed in the human genome (19,20). The prevalence of potential quadruplex forming sequences will depend on the guanine stretches and the nature of the loops. Trends in the sequence of the loops derived from a genome-wide survey of potential quadruplex sequences reveal that the loop length and its composition may determine the functionality of the quadruplexes and may modulate their role between genomes. Lately, a highly conserved potential quadruplex sequence upstream of *c-kit* has been found in human, mouse, rat and chimpanzee (21). G-stretches of potential quadruplex forming sequences in various protooncogenes are conserved but the regions interspersing these G-stretches, which form the loop of the quadruplex are not conserved. However, variation in loop length and composition affects quadruplex topology, stability (22–28) and its molecular recognition. This may modulate the function of the gene that harbors the potential quadruplex motif. In a genomic context, the guanine stretches are present along with their C-rich complementary strand, which generates a competition between a Hoogsteen bonded quadruplex and a Watson–Crick hydrogen bonded duplex. This quadruplex–duplex competition has been studied for

*To whom correspondence should be addressed. Tel: +91 11 2766 6156; Fax: +91 11 2766 7471; Email: souvik@igib.res.in

Table 1. Dual-labeled (5′ fluorescein and 3′ TAMRA) quadruplex forming sequences and their complementary sequences used in the study

G3T	5′ F TGGG T GGG T GGG T GGGT **T0** 3′
G3T2	5′ F TGGG TT GGG TT GGG TT GGGT **T0** 3′
G3T3	5′ F TGGG TTT GGG TTT GGG TTT GGGT **T0** 3′
G3T4	5′ F TGGG TTTT GGG TTTT GGG TTTT GGGT **T0** 3′
G3T5	5′ F TGGG TTTTT GGG TTTTT GGG TTTTT GGGT **T0** 3′
C3A	5′ ACCC A CCC A CCC A CCCA 3′
C3A2	5′ ACCC AA CCC AA CCC AA CCCA 3′
C3A3	5′ ACCC AAA CCC AAA CCC AAA CCCA 3′
C3A4	5′ ACCC AAAA CCC AAAA CCC AAAA CCCA 3′
C3A5	5′ ACCC AAAAA CCC AAAAA CCC AAAAA CCCA 3′

different sequences under various experimental conditions (29–41). Using telomeric oligonucleotides d[AGGG(TTAGGG)$_3$] and d[TCCC(AATCCC)$_3$], it has been shown that pH, temperature and salt concentration, controls the quadruplex-Watson Crick competition (33). Recently, we have reported the role of osmolytes and small molecule on quadruplex-Watson Crick competition (40). We found that these perturbants stabilize quadruplex and shift the equilibrium towards quadruplex formation.

Quadruplex-Watson Crick competition and the influence of the loops on quadruplex stability has been investigated separately, however, the role of loop length in modulating this competition still remains unaddressed. Herein, we address the role of loop length on the competition between quadruplex and duplex DNA. In the present study, we have used intramolecular quadruplex forming sequences, which have similar G-tracts but vary in their thymine loop length (T–T5). We compared the stability of these quadruplexes having different loop lengths with their respective duplexes, estimated the binding affinity and hybridization kinetics of these preformed quadruplexes towards their respective complementary strands, and observed the conformational fluctuations in the quadruplex conformers in the absence and presence of their respective complementary strands.

MATERIALS AND METHODS

Oligonucleotides and nomenclature

Unlabeled and dual-labeled (5′ Fluorescein and 3′ TAMRA) G-rich oligonucleotides and their respective complementary strand were procured from Sigma-Aldrich, Singapore. All the oligonucleotides were HPLC purified. The oligonucleotides used in this study are listed in Table 1.

The concentration of unlabeled oligonucleotide solutions was determined from the absorbance at 260 nm using a molar extinction coefficient for G-rich and C-rich strands, calculated by extrapolation of tabulated values of the monomers and dimers (42) at 25°C, using procedures reported earlier (43). The concentration of the labeled oligonucleotide was determined by measuring the absorbance of the attached fluorescein moiety at 496 nm using a molar extinction coefficient of $4.1 \times 10^4/\mathrm{M}^{-1}\mathrm{cm}^{-1}$ (44). All experiments were done in 50 mM MES buffer pH 7.4, 100 mM KCl. CD spectra were recorded in a Jasco spectropolarimeter (model 715, Japan) equipped with a thermoelectrically controlled cell holder and a cuvette with a path length of 1 cm. CD spectra for quadruplexes (5 μM) were recorded between 220 and 325 nm at 25°C in 50 mM MES buffer pH 7.4, 100 mM KCl. Equimolar concentration of quadruplexes (5 μM) and their respective complementary strands were incubated for 2 h at 25°C and CD spectra were recorded between 220 and 325 nm at 25°C in 50 mM MES buffer pH 7.4, 100 mM KCl.

Steady-state experiments

Fluorescence experiments were performed using Fluoromax 4 (spex) spectrofluorimeter and FLUOstar OPTIMA from BMG labtech (Germany). The excitation wavelength was set at 480 nm and the emission spectra were recorded from 500 to 700 nm. We collected temperature-dependent fluorescence cooling and heating curves for the quadruplexes alone and for equimolar mixture of each quadruplex and with its complementary strand at the rate of 0.2°C/min. These curves showed no hysteresis suggesting that the process is in thermodynamic equilibrium (SI). For clarity, we have only presented the cooling curves in the main text. Normalized donor (fluorescein) emission ($I_{520\,\mathrm{nm}} = F_t/F_{95}$) at 520 nm was plotted as a function of temperature, where F_t is the fluorescence at any temperature and F_{95} is the fluorescence at 95°C. The van't Hoff analysis was performed using the cooling profile of quadruplexes using a two state model for unstructured–structured transition to obtain the thermodynamic parameters for quadruplex formation (45).

A FLUOstar OPTIMA fluorescence plate reader was used to determine the binding affinity of each G-quadruplex to its complementary strand. The plate reader provides the advantage of working with many samples at very dilute concentrations and on systems that suffer from thermodynamic and kinetic inertia, and require prolonged incubation. The experiments were done in 384-well black plates, using excitation (480 nm) and emission (520 nm) filters for fluorescein. The wells were loaded with the solution of fixed concentration of preformed quadruplex (12 nM) and increasing concentrations of complementary strand (0–300 nM). Sample mixtures were incubated for a period of 24 h at 25°C, to ensure attainment of equilibrium and the plate was read at 520 nm. For analysis of the data, the observed fluorescence intensity was considered as the sum of the weighted contributions from a folded G-quadruplex strand and an extended G-strand:

$$F = (1 - \alpha_\mathrm{b})F_0 + \alpha_\mathrm{b}F_\mathrm{b} \qquad \mathbf{1}$$

where F is the observed fluorescence intensity at each titrant concentration, F_0 and F_b are the respective fluorescence intensities of initial and final states of titration, α_b is the mole fractions of quadruplex in duplex form. Assuming 1:1 stoichiometry for the interaction in case of complementary strand binding, it can be shown that:

$$[Q]_0\,\alpha_b^2 - \left([Q]_0 + [C]_0 + 1/K_\mathrm{A}\right)\alpha_\mathrm{b} + [C]_0 = 0 \qquad \mathbf{2}$$

where K_A is the association constant, $[Q]_0$ is the total G-strand concentration and $[C]_0$ is the added complementary strand concentration.

From Equations (1) and (2), it can be shown that:

$$\Delta F = \left(\frac{\Delta F_{max}}{2[Q]_0}\right)\left\{([Q]_0+[C]_0+1/K_A) - \sqrt{([Q]_0+[C]_0+1/K_A)^2-4[Q]_0[C]_0}\right\} \quad \textbf{3}$$

where $\Delta F = F - F_0$ and $\Delta F_{max} = F_{max} - F_0$

Kinetic experiments

The kinetic experiments were performed in a Fluoromax 4 (spex) spectrofluorimeter. The opening up of the quadruplex (30 nM) upon addition of an equivalent concentration of the complementary strand was monitored as the increase in the fluorescence intensity at 520 nm as a function of time. The data obtained for G3T were fit by a single exponential Equation (4a), whereas the kinetics data for other quadruplexes (G3T2–G3T5) required a double exponential kinetics Equation (4b) with good residuals (SI). The equation used was:

$$\Delta F = A_1 e^{-t/\Gamma_1} \quad \textbf{4a}$$

$$\Delta F = A_1 e^{-t/\Gamma_1} + A_2 e^{-t/\Gamma_2} \quad \textbf{4b}$$

where Γ_1 and Γ_2 are the time constants of the kinetics and A_1 and A_2 are their respective weighted amplitudes.

Fluorescence correlation spectroscopy

Fluorescence correlation spectroscopy (FCS) experiments were performed with a home-built spectrometer using single-photon excitation as described previously (46). Briefly, the experimental setup consists of a high-numerical aperture objective lens (60×, 1.2 NA, water immersion, Nikon, Melville, NY, USA), which focuses a continuous wave blue laser (Argon ion Laser 1.2 mW at 488 nm from LG Laser GmbH, Germany) into the sample. The laser power at the objective back aperture is kept typically <100 μW. Fluorescence is collected through the microscope objective separated from the excitation light by a dichroic mirror (DC 514, Chroma Inc., Brattleboro, VT, USA) and an emission filter (525DF30 DTM for the fluorescein and 585DF40 for Tamra, respectively Chroma Inc.), and focused with an achromatic lens (F = 150 mm, Newport, Irvine, CA, USA) onto a multimode fiber (25 μm core diameter, Newport). The other end of the fiber is connected to a fiber-coupled APD detector (SPCM-AQR-150, Perkin-Elmer, Fremont, CA, USA). The detector signal is then processed with an autocorrelator card (ALV5000E, ALV Laser VmbH, Langen, Germany). All FCS experiments were performed in 50 mM MES buffer pH 7.4, 100 mM KCl at 25°C at 100 nM concentration in presence and absence of equimolar concentration of complementary strands after 24 h of incubation. Autocorrelation profiles obtained for quadruplex for G3T fits to a single conformer model as shown in Equation (5), whereas quadruplexes G3T2–G3T5 fits to two conformer model as shown in Equation (6) (47,48). The autocorrelation function obtained for quadruplex G3T with its complementary strand fits to Equation (7), and quadruplexes (G3T2–G3T5) in presence of complementary strand fits to Equation (8).

$$G(\tau) = G_0\left(\frac{1}{1+(\tau/\tau_D)}\right)\left(\frac{1}{1+a^2(\tau/\tau_D)}\right)^{1/2} \quad \textbf{5}$$

$$G(\tau) = \frac{1-F+F\exp(\tau/\tau_R)}{N(1-F)}\left(\frac{1}{1+(\tau/\tau_D)}\right)\left(\frac{1}{1+a^2(\tau/\tau_D)}\right)^{1/2} \quad \textbf{6}$$

$$G(\tau) = G_1\left(\frac{1}{1+(\tau/\tau_{D1})}\right)\left(\frac{1}{1+a^2(\tau/\tau_{D1})}\right)^{1/2} + G_2\left(\frac{1}{1+(\tau/\tau_{D2})}\right)\left(\frac{1}{1+a^2(\tau/\tau_{D2})}\right)^{1/2} \quad \textbf{7}$$

$$G(\tau)=\left[\frac{1-F+F\exp(\tau/\tau_R)}{N(1-F)}\right]G_1\left(\frac{1}{1+(\tau/\tau_{D1})}\right)\left(\frac{1}{1+a^2(\tau/\tau_{D1})}\right)^{1/2}+G_2\left(\frac{1}{1+(\tau/\tau_{D2})}\right)\left(\frac{1}{1+a^2(\tau/\tau_{D2})}\right)^{1/2} \quad \textbf{8}$$

where F is the dark fraction, N is the number of particles, τ_R is the time scale of internal conformational fluctuation, τ_D and τ_{D1} is the diffusion time of quadruplex, τ_{D2} is the diffusion time of duplex and a is the ratio of radial to axial distance of the probe volume. G_1 and G_2 are the fraction of population weighted by the square of the brightness.

RESULTS

CD spectra provide valuable information about the structural transitions in nucleic acids. We therefore recorded the spectra of quadruplexes with similar G stretches but varied loop length (T–T5) in the absence and presence of their respective complementary strands. The G3T quadruplex has a parallel conformation with characteristic positive and negative peaks at 262 and 240 nm, respectively (Figure 1a). In case of G3T2 and G3T3, there was a positive peak at 262 nm, a small positive peak at 292 nm and a negative peak at 237 nm, suggesting the presence of a predominant parallel quadruplex and a small fraction of antiparallel population (Figure 1b and c). Further increase in the loop length for G3T4 and G3T5, resulted in a positive peak at 292 nm, a relatively small positive peak at 260 nm, and a negative peak at 238 nm, indicating the presence of a predominant antiparallel quadruplex with a small parallel population (Figure 1d and e). The addition of an equimolar concentration of the complementary strand to the preformed G3T quadruplex,

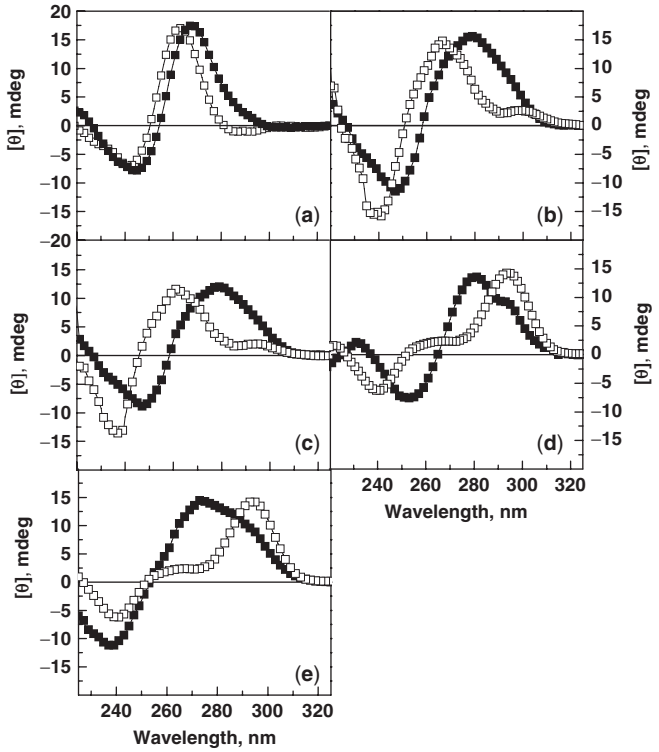

Figure 1. CD spectra of quadruplex (5 μM) in absence (open square) and presence of equimolar complementary strand (filled square) recorded in 50 mM MES buffer pH 7.4, 100 mM KCl at 25°C for (**a**) G3T, (**b**) G3T2, (**c**) G3T3, (**d**) G3T4 and (**e**) G3T5.

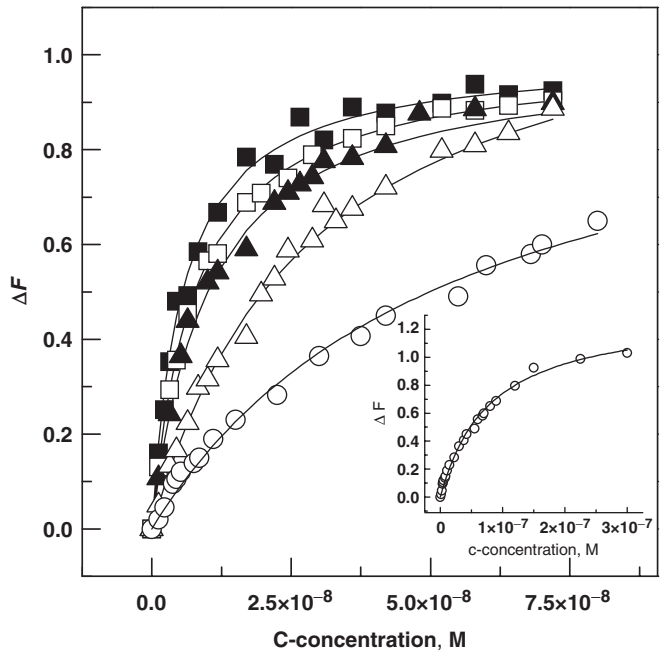

Figure 2. Opening of quadruplexes formed G3T (open circle), G3T2 (open triangle), G3T3 (filled triangle), G3T4 (open square) and G3T5 (filled square) in presence of different concentrations of complementary strand in 50 mM MES buffer pH 7.4, 100 mM KCl at 25°C. Inset shows the opening of quadruplex formed G3T (open circle) in presence of different concentrations of complementary strand in 50 mM MES buffer pH 7.4, 100 mM KCl at 25°C. Fluorescence change reflects quadruplex hybridization to its complementary strand for duplex formation.

resulted in only a moderate shift in the positive and negative peaks to 267 and 245 nm, respectively, suggesting minor duplex formation. Similar additions of equimolar concentrations of respective complementary strands to preformed G3T2 and G3T3 quadruplexes led to the substantial loss of the small band at 292 nm, and a prominent shift in positive and negative peaks. The broad positive peak obtained at 277 nm and the negative peak at 246 nm suggests duplex formation with some contribution from a residual parallel quadruplex population (Figure 1b and c). Addition of equimolar complementary strands to preformed G3T4 and G3T5 quadruplexes resulted in the prominent shift in the positive peak from 292 to 280 nm and a shift of the negative peak from 238 to 246 nm, which indicates duplex formation. However, a broad shoulder base around 290 nm still exists, suggesting the presence of certain fraction of quadruplex in the solution (Figure 1d and e).

Next, we assessed the influence of loop length on the quadruplex to duplex transition by determining the binding affinity of quadruplexes towards their respective complementary strand through FRET. When a quadruplex opens in presence of its complementary strand, the distance between the donor and acceptor increases. This results in reduced energy transfer from the donor to the acceptor and an increase in donor signal. We monitored the fluorescence of fluorescein with increasing complementary strand concentration for all the sequences used in this study. Figure 2 represents the relative fluorescence intensity change (ΔF) as function of the complementary strand concentration. The difference in profile of relative fluorescence intensity change (ΔF) obtained for quadruplexes with different loop length reflects the amount of duplex formed upon hybridization of quadruplex to its complementary strand. We observed that the quadruplex formed by G3T required approximately 25 times excess of complementary strand for maximum duplex formation (Inset Figure 2), whereas other quadruplexes G3T2–G3T5 required approximately 6 times excess of complementary strand for maximum duplex formation. The plot represented in Figure 2 was used to calculate the binding affinity of quadruplexes to their complementary strands using Equation (3). The binding affinity towards the complementary strands at 25°C is shown in Table 2. Next, we followed the kinetics of duplex formation, which involves the unfolding of quadruplex and hybridization to its complementary strand at 25°C in 100 mM KCl. Data analysis shows that the kinetics of duplex formation for G3T follows a single exponential with mean time constant of 9896 s. However, for quadruplexes G3T2–G3T5, best fitting results required a double exponential kinetics model, which reveals the presence of atleast two quadruplex conformers having different duplex formation kinetics (SI). Using Equation (4b), we obtained the relative proportions of quadruplex conformers and their respective time constant values (Table 2). Data analysis shows that duplex formation involves a contribution from a predominant slow opening conformer and small population of fast

Table 2. Thermodynamic and kinetic parameters obtained from experiments conducted at 25°C in 50 mM MES buffer pH 7.4, 100 mM KCl

	A_1	A_2	Γ_1 (s)	Γ_2 (s)	K_A (M^{-1})	Q_f (nM)	D_{eq} (nM)
G3T	0.94	–	9896 ± 100	–	$1.0\times10^7 \pm 0.5$	24.2	5.8
G3T2	0.88	0.12	9614 ± 115	1415 ± 135	$3.4\times10^7 \pm 0.5$	18.6	11.4
G3T3	0.70	0.30	6510 ± 125	1080 ± 98	$9.6\times10^7 \pm 0.7$	13.2	16.8
G3T4	0.72	0.28	6120 ± 108	747 ± 50	$1.3\times10^8 \pm 0.2$	11.7	18.3
G3T5	0.66	0.34	2920 ± 150	364 ± 65	$1.7\times10^8 \pm 0.3$	10.7	19.3

The kinetics of duplex formation for G3T quadruplex fits to single exponential kinetics, whereas data for quadruplexes G3T2–G3T5 fits to biexponential kinetics. A_1 and A_2 are weighted fractions of quadruplex population hybridizing to complementary strand with their respective Γ_1 and Γ_2 time constant values. K_A is the equilibrium constant for duplex formation. Q_f and D_{eq} is free quadruplex and duplex concentration, when equimolar concentration of quadruplex and complementary strand (30 nM) are mixed together in 50 mM MES buffer pH 7.4, 100 mM KCl. The amount of duplex at equilibrium, D_{eq}, was calculated from the binding affinity towards the complementary strand obtained from different experimental conditions, using the equation $K_A = D_{eq}/(Q_0-D_{eq}) \times (C_0-D_{eq})$, where Q_0 and C_0 ($Q_0 = C_0$) are the initial quadruplex and complementary strand concentration.

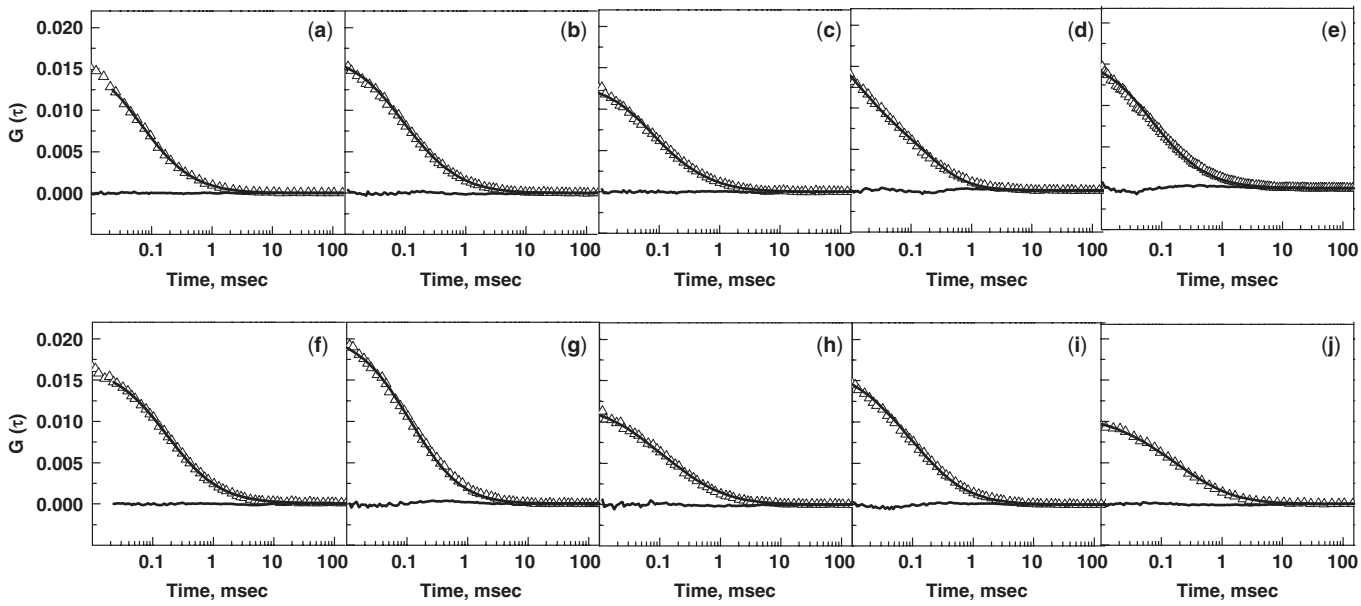

Figure 3. Autocorrelation profiles along with their residuals determined for quadruplex alone (**a–e**) and for equimolar mixture of quadruplex and respective complementary strand (**f–j**) in 50 mM MES buffer pH 7.4, 100 mM KCl for G3T, G3T2, G3T3, G3T4 and G3T5.

opening conformer. The time constants obtained for the slow and fast opening conformer are tabulated in Table 2.

We next investigated the dynamic behavior and conformational heterogeneity in a quadruplex–duplex population using FCS (46). This technique allows analysis of spontaneous fluctuations in the fluorescence signal arising in a microscopic volume of fluorescent sample. These fluctuations arise due to hydrodynamic processes like diffusion and biophysical process like conformational fluctuations (49–55). Therefore, in principle this technique can be employed to understand the influence of loop length on dynamic fluctuations in quadruplex structure during the quadruplex-Watson Crick duplex transition. We performed FCS measurements for quadruplexes with similar G-stretches with varying loop length (T–T5). The autocorrelation function for G3T fits to a single diffusing conformer Equation (5) with diffusion time (τ_D) value of 0.095 ms. Interestingly, the autocorrelation function for quadruplexes (G3T2–G3T5) did not fit to a single diffusion equation, suggesting the existence of more than one conformer undergoing conformational transformations. These conformational motions between interconverting conformers may not substantially affect the overall hydrodynamic radius, but demonstrate variation in FRET efficiency due to difference in donor and acceptor distance. Therefore, we used Equation (6), which allows estimation of reaction time (τ_R) and diffusion time (τ_D), and fits an autocorrelation function with reasonable residuals, as shown in Figure 3a–e. The τ_R in Equation (6) corresponds to the time scale for conformational fluctuations in the quadruplex and τ_D corresponds to the diffusion time of the quadruplex through a small observation area. The analysis of FCS data shows an increase in the diffusion time (τ_D) from 0.133 to 0.164 ms when the loop length is increased from T2 to T5 with a corresponding increase in the conformational fluctuation (τ_R) from 0.062 to 0.093 ms (Table 3). The τ_R and τ_D values obtained from Equation (6) were derived with the assumption

Table 3. Fluorescence correlation spectroscopy measurements conducted in 50 mM MES buffer pH 7.4, 100 mM KCl at 25°C

	Quad		Quad + Complementary strand		
	τ_R (ms)	τ_{D1} (ms)	τ_R (ms)	τ_{D1} (ms)	τ_{D2} (ms)
G3T	–	0.095 ± 0.012	–	0.088 ± 0.008	0.198 ± 0.010
G3T2	0.062 ± 0.003	0.133 ± 0.008	0.059 ± 0.003	0.105 ± 0.004	0.232 ± 0.004
G3T3	0.070 ± 0.003	0.138 ± 0.011	0.042 ± 0.003	0.135 ± 0.003	0.253 ± 0.003
G3T4	0.082 ± 0.002	0.152 ± 0.002	0.035 ± 0.002	0.140 ± 0.003	0.285 ± 0.006
G3T5	0.093 ± 0.003	0.164 ± 0.002	0.030 ± 0.002	0.172 ± 0.004	0.298 ± 0.005

G3T quadruplex adopts only one conformer and data obtained for G3T in absence and presence of complementary strand were fit to Equations (5) and (7) (Materials and methods section), respectively. Quadruplexes G3T2–G3T5 adopts two conformers, and the data obtained in absence and presence of their complementary strands were fit to Equations (6) and (8) (Materials and Methods section), respectively. Where τ_R is the time scale of conformational fluctuation in quadruplex, τ_D and τ_{D1} is the diffusion time of quadruplex, τ_{D2} is the diffusion time of duplex.

that $\tau_R \ll \tau_D$. But this is not observed here, as τ_R and τ_D values show a difference of ~2-fold. We accept that if τ_D and τ_R are close, then the diffusion and the reaction kinetic region in the autocorrelation function are not easily separable. However, for the case when the diffusion constants of the two species are nearly equal, the separation remains a reasonable approximation, as pointed out by Torres and Levitus (54). Further, FCS experiments were performed to investigate the influence of complementary strand on the interconversion amongst the quadruplex conformers while driving duplex formation. An equimolar solution of dual-labeled quadruplex and its complementary strand would have two fluorescent populations corresponding to the quadruplex and duplex species, which are expected to have different FRET efficiencies and diffusion time (Figure 3f–j). G3T adopts a single quadruplex conformation and its autocorrelation function in presence of complementary strand fits to Equation (7). Here, we assume that the duplex has only one conformation and the estimated τ_{D1} and τ_{D2} value correspond to the diffusion time of the quadruplex and duplex structure, respectively. We observed that the τ_{D1} value was 0.088 ms and τ_{D2} value was 0.198 ms. However, the autocorrelation function obtained for G3T2–G3T5 quadruplexes in presence of their respective complementary strands fits to Equation (8) which provides τ_R, τ_{D1} and τ_{D2} values that correspond to the conformational fluctuation within the conformers in quadruplex structure, diffusion time of the quadruplex and duplex structure, respectively. We observed that the τ_{D1} values increased from 0.105 to 0.172 ms and the τ_{D2} values increased from 0.232 to 0.298 ms with increase in loop length from T2 to T5. Interestingly, the τ_R values, which correspond to the conformational fluctuations in the quadruplex structure decreased from 0.059 to 0.030 ms with increase in the loop length. This suggests the increase in fluctuations among the quadruplex conformers in presence of complementary strand, especially for quadruplex with longer loop length.

We also analyzed the role of loop length on the relative stability of quadruplex and duplex, which affect the fate of the competition. The fluorescence cooling profile would involve the contribution from quadruplex, duplex and random coil populations with the relative trend in the donor fluorescence signals as duplex> random coil> quadruplex. The cooling profile of the quadruplex alone shows the expected sigmoidal curve except for G3T, which melts at temperature >85°C. However, the cooling curves obtained for the equimolar concentration of both the strands exhibited the quadruplex cooling profile at higher temperature but with further decrease in temperature, the fluorescence signal increases as shown in Figure 4. The fluorescence intensity change obtained at temperatures >90°C represents predominantly random coil contribution. Decrease in temperature results in an initial decrease followed by subsequent increase in fluorescence intensity, which corresponds to the quadruplex and duplex formation, respectively. The relative stability of the competing quadruplex and duplex structures would thereby dictate the predominance of either of the structures, and consequently affect the fluorescence change at 20°C. Figure 4 depicts that the fluorescence intensity at

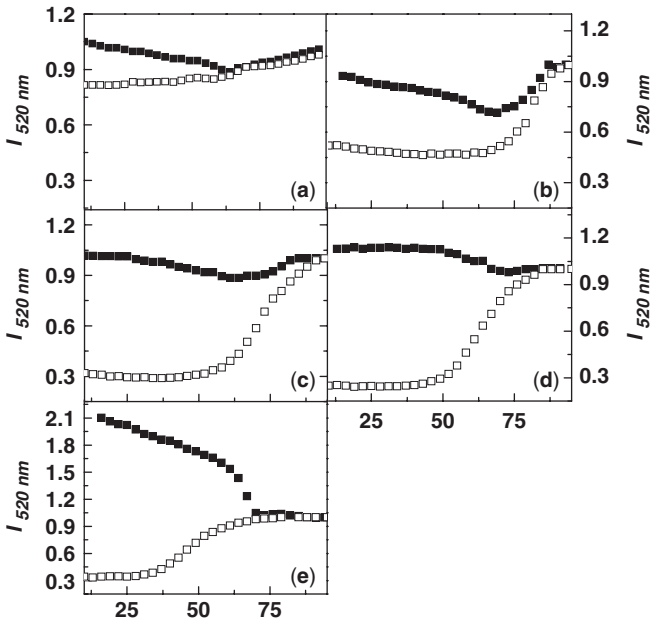

Figure 4. Fluorescence cooling curves for quadruplexes formed (**a**) G3T, (**b**) G3T2, (**c**) G3T3, (**d**) G3T4 and (**e**) G3T5 in absence (open square) and presence (filled square) of equimolar concentration (30 nM) of complementary strand in 50 mM MES buffer, pH 7.4 100 mM KCl with cooling rate of 0.2°C/min.

Table 4. Experimental and predicted thermodynamic parameters obtained for the quadruplex and duplex formation

	Quadruplex[a]				Duplex[b]			
	T_m°C	ΔH° kcal/mol	ΔS° cal/mol/K	ΔG°_{25} kcal/mol	T_m°C	ΔH° kcal/mol	ΔS° cal/mol/K	ΔG°_{25} kcal/mol
G3T	-	–	–	–	60.4	−127	−335	−24.2
G3T2	82	−44	−121	−8.0	61.7	−151	−414	−27.2
G3T3	71	−36	−105	−4.7	62.7	−174	−483	−30.4
G3T4	63	−33	−97	−4.1	63.4	−198	−552	−33.2
G3T5	46	−31	−95	−2.7	64.0	−222	−622	−36.3

[a]Fluorescence cooling profile of quadruplex (30 nM) obtained in 50 mM MES buffer, 100 mM KCl, pH 7.4. The thermodynamic parameters for the G3T quadruplex could not be determined due high thermal stability of structure, which melts at temperatures >85°C. T_m values are within ±1°C error. van't Hoff analysis performed for fluorescence cooling profile to obtained thermodynamic parameters. ΔH°, ΔS° and ΔG° is within 10% error.

[b]Predicted thermodynamic parameters for the duplex formed by all sequences obtained through HYTHER (ozone2.chem.wayne.edu) using experimental conditions of 30 nM strand concentration and 100 mM monovalent cations.

lower temperature (20°C) for an equimolar mixture of G-rich and C-rich strand varies for quadruplexes with different loop length. We observed an increase in the fluorescence intensity at 20°C with increase in loop length (T2–T5). This increase in the intensity was found to be maximum for G3T5 and minimum for G3T, indicating maximum duplex formation for G3T5 and minimum for G3T.

We determined the thermodynamic profile of quadruplex formation through fluorescence cooling curves (SI). The thermodynamic parameters for quadruplex formation were obtained using a two-state model for unstructured–structured transition, assuming that a major contribution is from the predominant population only. Since it is difficult to obtain the thermodynamic parameters for quadruplex from spectroscopic measurements with high precision, therefore, we have drawn qualitative trends from this analysis. The thermodynamic parameters for the G3T quadruplex could not be determined due to high thermal stability of the structure, which melts at temperatures >85°C, and is in agreement with previous report (22). Data analysis for unstructured–structure transition of quadruplexes show that the enthalpy and entropy vary from −44 to –31 kcal/mol and −121 to –95 cal/mol/K for G3T2 to G3T5, respectively (Table 4). However, the fluorescence cooling curves obtained for an equimolar G-rich and C-rich strand involves the contribution from random coil, quadruplex and duplex, and hence cannot be used to obtain the thermodynamic profile the of duplex. Therefore, we evaluated the thermodynamic profile for the duplex through the nearest neighbor (NN) method. During past decades numerous studies have been performed to calculate the thermodynamic parameters of a given duplex under specified experimental conditions by this method. It is well established that the NN method allows evaluation of the thermal stability and the thermodynamic parameters of duplexes with high precision and the obtained results are in agreement with the experimental data. Hyther (56,57) is a tool that allows calculation of nucleic acid hybridization thermodynamics using the NN method. Using Hyther, we predicted the thermodynamic profile of duplexes formed by the G-rich sequence with their respective complementary strand at experimental strand concentration and buffer conditions (Table 4). We observed that during duplex formation, for T–T5, the enthalpy and entropy varies from −127 to −222 kcal/mol and −335 to −622 cal/mol/K, respectively. The thermodynamic stability of duplexes was calculated to increase from –24.2 kcal/mol to –36.3 kcal/mol upon increasing the loop length from T to T5 (Table 4).

DISCUSSION

To understand the role of loop length on the quadruplex–duplex competition, we determined the binding affinity of preformed quadruplexes to their complementary strands, and obtained the following trend G3T < G3T2 < G3T3 < G3T4 < G3T5. The change in binding affinity obtained upon increasing the loop length from T to T5 is not very large ($1.0 \times 10^7\,M^{-1}$ to $1.7 \times 10^8\,M^{-1}$), resulting in a difference of ∼1.7 kcal/mol in ΔG° value for duplex formation. However, the ΔG° for quadruplex formation varied from −8.0 kcal/mol to –2.7 kcal/mol with increase in loop length from T2 to T5 (Table 4). As the loop length has opposite effects on the thermodynamic stability of quadruplexes and duplexes, the important parameter that would dictate the predominance of either of the population (duplex or quadruplex) is the relative free energy difference, the $\Delta\Delta G^\circ_{25}$ between the duplex and quadruplex structure, and not the ΔG°_{25} alone. $\Delta\Delta G^\circ_{25}$ increases in magnitude upon increasing the loop length from −2.2 kcal/mol to −8.5 kcal/mol for G3T2 and G3T5, respectively. The greater negative magnitude of $\Delta\Delta G^\circ_{25}$ implies that the competition favors duplex formation, as in case of T5. Further, this predominance of duplex is strongly competed by the quadruplex on decreasing the loop length.

Our kinetic data reveal the presence of one conformer for G3T quadruplex and two conformers for quadruplexes G3T2–G3T5, which unfold at different rates in presence of their complementary strands. The presence of two conformers (parallel and antiparallel structures) is also supported by our CD study. The conformers contributing towards duplex formation include a predominant slow opening conformer and a small population of fast opening

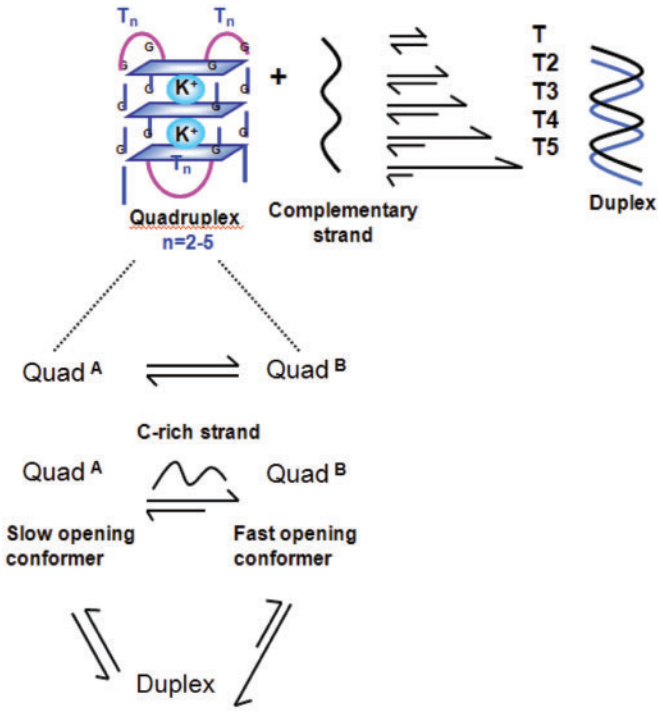

Figure 5. Mechanism for duplex formation involving quadruplex with loop length varying from T to T5. Duplex formation increases with increase in loop length from T to T5. Quadruplex structures with loop length T2 to T5 involve two interconverting conformers ($Quad^A$ and $Quad^B$). In presence of complementary strand, equilibrium between the two conformers is shifted towards faster opening conformer $Quad^B$, which facilitates hybridization to complementary strand for duplex formation.

conformer. We observe increase in the population of fast opening conformer when the loop length is increased from T2-T5 (Table 2), which additionally contributes to faster duplex formation. Similarly, NMR study has shown the coexistence of interconverting parallel and antiparallel quadruplex structures for human telomeric sequence (58). These conformers have different kinetics of unfolding in presence of complementary strand resulting in double exponential parameters for Watson–Crick duplex formation (58). We performed FCS to investigate the influence of loop length on the interconversion between the quadruplex conformers during the quadruplex–duplex competition. The sequences with loop length T2–T5, adopt different topologies resulting in different τ_D values and these values increase with an increase in loop length. We observed that G3T adopts only one conformation and is in agreement with our CD and kinetics result. Whereas, the quadruplexes G3T2–G3T5 adopt two diffusible conformers which have similar hydrodynamic radii. The interconversion between these conformers decrease with increase in loop length from T2 to T5. This can be attributed to the intramolecular stacking of loop residues which retard the internal molecular motions within the interconverting quadruplex conformers with longer loops. Similar conformational diversity has also been reported for telomeric quadruplex having conformers with different FRET efficiencies (36,41,55). The FCS measurements performed for the equimolar mixture of quadruplexes and their complementary strands show increase in the diffusion time for both quadruplex and duplex structure upon increase in loop length. We also observe a concomitant increase in the interconversion between the conformers in presence of the complementary strand. Correlating our fluorescence binding, kinetic and FCS study, an elementary scheme for duplex formation has been proposed in Figure 5. As illustrated in Figure 5, we primarily observe increase in duplex formation upon increase in loop length of quadruplex. The quadruplex structures adopted by G3T2–G3T5 comprise of two conformers having specific interconversion rate. Loop length of quadruplex structure can modulate the interconversion between these conformers in absence and presence of the complementary strand. The quadruplex structure includes a predominant slow opening conformer and a small population of fast opening conformer, both contributing to duplex formation with different hybridization rates. In presence of the complementary strand, the interconversions between the conformers increase with an increase in loop length. This shifts the equilibrium between the conformers towards the fast opening population, and thereby facilitating hybridization to the complementary strand for duplex formation.

Using the equilibrium binding constants obtained in this study for quadruplexes towards their complementary strands, we calculated the fraction of free quadruplex (Q_f) and the amount of duplex formed (D_{eq}) at equilibrium, as shown in Table 2. We found that for an equimolar mixture (30 nM) of quadruplex and its complementary strand in 100 mM KCl buffer, duplex population increases with increase in the loop length. Duplex is predominant in case of G3T5, in contrast to G3T which has a predominant quadruplex population. The duplex concentration obtained under the experimental conditions at equilibrium was 5.8, 11.4, 16.8, 18.3 and 19.3 nM for G3T, G3T2, G3T3, G3T4 and G3T5, respectively, (Table 2). Comparing our earlier study on G3TTA (40) and the current study, it is observed that the duplex formed at equilibrium by G3TTA and G3T3 is 12.4 and 16.8 nM, respectively. Replacing adenine residue in G3TTA with thymine probably could affect the loop topology and allow better hybridization to the complementary strand, and thus shift the equilibrium to favor duplex formation. These observations give insight into the role of loop length in modulating the predominance of the competing secondary structures and perturbing the dynamic equilibrium between the quadruplex and duplex.

CONCLUSION

Loop length and its composition have vital influence on conformation, stability and on the structural competition between the quadruplex and Watson–Crick duplex. The relative stability of the duplex and quadruplex structure would dictate the predominance of either of these structures at equilibrium. Our results unambiguously reinforce that the increase in the loop length of the potential quadruplex forming sequence favors duplex formation and outcompetes the quadruplex.

SUPPLEMENTARY DATA

Supplementary Data are available at NAR Online.

ACKNOWLEDGEMENTS

N.K. acknowledges CSIR for fellowship. S.M. acknowledges CSIR for funding this research. We thank 'The Centre for Genomics Applications, (TCGA)' at IGIB granted by CSIR and DST for providing instrumental facility and technical help. Funding to pay the Open Access publication charges for this article was provided by CSIR, India.

Conflict of interest statement. None declared.

REFERENCES

1. Gellert,M., Lipsett,M.N. and Davies,D.R. (1962) Helix formation by guanylic acid. *Proc. Natl Acad. Sci. USA*, **48**, 2013–2018.
2. Balagurumoorthy,P. and Brahmachari,S.K. (1994) Structure and stability of human telomeric sequence. *J. Biol. Chem.*, **269**, 21858–21869.
3. Pinnavaia,T.J., Marshall,C.L., Mettler,C.M., Fisk,C.L., Miles,H.T. and Becker,E.D. (1978) Alkali metal ion specificity in the solution ordering of a nucleotide, 5′-guanosine monophosphate. *J. Am. Chem. Soc.*, **100**, 3625–3627.
4. Blackburn,E.H. (1994) Telomeres: no end in sight. *Cell*, **77**, 621–623.
5. Sen,D. and Gilbert,W. (1988) Formation of parallel four-stranded complexes by guanine-rich motifs in DNA and its implications for meiosis. *Nature*, **334**, 364–366.
6. Maizels,N. (2006) Dynamic roles for G4 DNA in the biology of eukaryotic cells. *Nat. Struct. Mol. Biol.*, **13**, 1055–1059.
7. Huppert,J.L. (2008) Hunting G-quadruplexes. *Biochimie* [Epub ahead of print; 6 Feb 2008] doi:10.1016/j.biochi.2008.01.014.
8. Ghosal,G. and Muniyappa,K. (2006) Hoogsteen base-pairing revisited: resolving a role in normal biological processes and human diseases. *Biochem. Biophys. Res. Commun*, **343**, 1–7.
9. Fry,M. (2007) Tetraplex DNA and its interacting proteins. *Front Biosci*, **12**, 4336–4351.
10. Fang,G. and Cech,T.R. (1993) Characterization of a G-quartet formation reaction promoted by the beta-subunit of the Oxytricha telomere binding protein. *Biochemistry*, **32**, 11646–11657.
11. Giraldo,R., Suzuki,M., Chapman,L. and Rhodes,D. (1994) Promotion of parallel DNA quadruplexes by a yeast telomere binding protein: a circular dichroism study. *Proc. Natl Acad. Sci. USA*, **91**, 7658–7662.
12. Muniyappa,K., Anuradha,S. and Byers,B. (2000) Yeast meiosis-specific protein Hop1 binds to G4 DNA and promotes its formation. *Mol. Cell. Biol.*, **20**, 1361–1369.
13. Ghosal,G. and Muniyappa,K. (2005) *Saccharomyces cerevisiae* Mre11 is a high-affinity G4 DNA-binding protein and a G-rich DNA-specific endonuclease: implications for replication of telomeric DNA. *Nucleic Acids Res.*, **33**, 4692–4703.
14. Liu,Z. and Gilbert,W. (1994) The yeast KEM1 gene encodes a nuclease specific for G4 tetraplex DNA: implication of in vivo functions for this novel DNA structure. *Cell*, **77**, 1083–1092.
15. Sun,H., Yabuki,A. and Maizels,N. (2001) A human nuclease specific for G4 DNA. *Proc. Natl Acad. Sci. USA*, **98**, 12444–12449.
16. Huber,M.D., Lee,D.C. and Maizels,N. (2002) G4 DNA unwinding by BLM and Sgs1p: substrate specificity and substrate-specific inhibition. *Nucleic Acids Res.*, **30**, 3954–3961.
17. Sun,H., Karow,J.K., Hickson,I.D. and Maizels,N. (1998) The Bloom's syndrome helicase unwinds G4 DNA. *J. Biol. Chem.*, **273**, 27587–27592.
18. Fry,M. and Leob,L.A. (1999) Human werner syndrome DNA helicase unwinds tetrahelical structures of the fragile X syndrome repeat sequence d(CGG)n. *J. Biol. Chem.*, **274**, 12797–12802.
19. Huppert,J.L. and Balasubramanian,S. (2005) Prevalence of quadruplexes in the human genome. *Nucleic Acids Res.*, **33**, 2908–2916.
20. Todd,A.K., Johnston,M. and Neidle,S. (2005) Highly prevalent putative quadruplex sequence motifs in human DNA. *Nucleic Acids Res.*, **33**, 2901–2907.
21. Fernando,H., Reszka,A.P., Huppert,J.L., Ladame,S., Rankin,S., Venkitaraman,A.R., Neidle,S. and Balasubramanian,S. (2006) A conserved quadruplex motif located in a transcription activation site of the human c-kit oncogene. *Biochemistry*, **45**, 7854–7860.
22. Hazel,P., Huppert,J.L., Balasubramanian,S. and Neidle,S. (2004) Loop-length-dependent folding of G-quadruplexes. *J. Am. Chem. Soc.*, **126**, 16405–16415.
23. Hazel,P., Parkinson,G.N. and Neidle,S. (2006) Predictive modelling of topology and loop variations in dimeric DNA quadruplex structures. *Nucleic Acid Res.*, **34**, 2117–2127.
24. Smirnov,I. and Shafer,R.H. (2000) Effect of loop sequence and size on DNA aptamer stability. *Biochemistry*, **39**, 1462–1468.
25. Rachwal,P.A., Findlow,I.S., Werner,J.M., Brown,T. and Fox,K.R. (2007) Intramolecular DNA quadruplexes with different arrangements of short and long loops. *Nucleic Acid Res.*, **35**, 4214–4222.
26. Guédin,A., De Cian,A., Gros,J., Lacroix,L. and Mergny,J. L. (2008) Sequence effects in single-base loops for quadruplexes. *Biochimie*, **90**, 686–696.
27. Rachwal,P.A., Brown,T. and Fox,K.R. (2007) Sequence effects of single base loops in intramolecular quadruplex DNA. *FEBS Lett.*, **44**, 1657–1660.
28. Bugaut,A. and Balasubramanian,S. (2008) A sequence-independent study of the influence of short loop lengths on the stability and topology of intramolecular DNA G-quadruplexes. *Biochemistry*, **47**, 689–697.
29. Miura,T. and Thomas,G.J. (1994) Structural polymorphism of telomere DNA: interquadruplex and duplex-quadruplex conversions probed by Raman spectroscopy. *Biochemistry*, **33**, 7848–7856.
30. Deng,H. and Braunlin,W.H. (1995) Duplex to quadruplex equilibrium of the self-complementary oligonucleotide d(GGGGCCCC). *Biopolymers*, **35**, 677–681.
31. Kumar,N. and Maiti,S. (2004) Quadruplex to Watson-Crick duplex transition of the thrombin binding aptamer: a fluorescence resonance energy transfer study. *Biochem. Biophys. Res. Commun.*, **319**, 759–767.
32. Datta,B. and Armitage,B.A. (2001) Hybridization of PNA to structured DNA targets: quadruplex invasion and the overhang effect. *J. Am. Chem. Soc.*, **123**, 9612–9619.
33. Phan,A.T. and Mergny,J.L. (2002) Human telomeric DNA: G-quadruplex, i-motif and Watson–Crick double helix. *Nucleic Acids Res.*, **30**, 4618–4625.
34. Li,W., Wu,P., Ohmichia,T. and Sugimotoa,N. (2002) Characterization and thermodynamic properties of quadruplex/duplex competition. *FEBS Letters*, **526**, 77–81.
35. Green,J.J., Ying,L., Klenerman,D. and Balasubramanian,S. (2003) Kinetics of unfolding the human telomeric DNA quadruplex using a PNA trap. *J. Am. Chem. Soc.*, **125**, 3763–3767.
36. Ying,L., Green,J.J., Li,H., Klenerman,D. and Balasubramanian,S. (2003) Studies on the structure and dynamics of the human telomeric G quadruplex by single-molecule fluorescence resonance energy transfer. *Proc. Natl Acad. Sci. USA*, **100**, 14629–14634.
37. Risitano,A. and Fox,K.R. (2003) Stability of intramolecular DNA quadruplexes: comparison with DNA duplexes. *Biochemistry*, **42**, 6507–6513.
38. Kumar,N. and Maiti,S. (2007) Role of locked nucleic acid modified complementary strand in quadruplex/Watson-Crick duplex equilibrium. *J. Phys. Chem. B.*, **111**, 12328–12337.
39. Li,W., Miyoshi,D., Nakano,S. and Sugimoto,N. (2003) Competition involving G-quadruplex DNA and its complement. *Biochemistry*, **42**, 11736–11744.
40. Kumar,N. and Maiti,S. (2005) The effect of osmolytes and small molecule on quadruplex–WC duplex equilibrium: a fluorescence resonance energy transfer study. *Nucleic Acid Res.*, **33**, 6723–6732.
41. Shirude,P.S., Okumus,B., Ying,L., Ha,T. and Balasubramanian,S. (2007) Single-molecule conformational analysis of G-quadruplex formation in the promoter DNA duplex of the proto-oncogene C-kit. *J. Am. Chem. Soc.*, **129**, 7484–7485.
42. Cantor,C.R., Warshaw,M.M. and Shapiro,H. (1970) Oligonucleotide interactions. 3. Circular dichroism studies of the conformation of deoxyoligonucleotides. *Biopolymers*, **9**, 1059–1077.

43. Marky,L.A., Blumenfeld,K.S., Kozlowski,S. and Breslauer,K.J. (1983) Salt-dependent conformational transitions in the self-complementary deoxydodecanucleotide d(CGCAATTCGCG): evidence for hairpin formation. *Biopolymers*, **9**, 1247–1257.
44. Sjöback,R., Nygren,J. and Kubista,M. (1998) Characterization of fluorescein-oligonucleotide conjugates and measurement of local electrostatic potential. *Biopolymers*, **464**, 445–453.
45. Marky,L.A. and Breslauer,K.J. (1987) Calculating thermodynamic data for transitions of any molecularity from equilibrium melting curves. *Biopolymers, **26**,* 1610–1620
46. Sengupta,P., Balaji,J. and Maiti,S. (2002) Measuring diffusion in cell membranes by fluorescence correlation spectroscopy. *Methods*, **27**, 374–387.
47. Widengren,J., Rigler,R. and Mets,U. (1994) Triplet state monitoring by fluorescence correlation spectroscopy. *J. Fluorescence*, **4**, 255–258.
48. Haupts,U., Maiti,S., Schwille,P. and Webb,W.W. (1998) Dynamics of fluorescence fluctuations in green fluorescent protein observed by fluorescence correlation spectroscopy. *Proc. Natl Acad. Sci. USA*, **95**, 13573–13578.
49. Magde,D., Elson,E.L. and Webb,W.W. (1974) Fluorescence correlation spectroscopy. II. An experimental realization. *Biopolymers*, **13**, 29–61.
50. Magde,D., Webb,W.W. and Elson,E.L. (1978) Fluorescence correlation spectroscopy. III. Uniform translation and laminar flow. *Biopolymers*, **1**, 361–376.
51. Bonnet,G., Krichevsky,O. and Libchaber,A. (1998) Kinetics of conformational fluctuations in DNA hairpin-loops. *Proc. Natl Acad. Sci. USA*, **95**, 8602–8606.
52. Wallace,M.I., Ying,L., Balasubramanian,S. and Klenerman,D. (2001) Non-Arrhenius kinetics for the loop closure of a DNA hairpin. *Proc. Natl Acad. Sci. USA*, **98**, 5584–5589.
53. Bonnet,G., Tyagi,S., Libchaber,A. and Kramer,F.R. (1999) Thermodynamic basis of the enhanced specificity of structured DNA probes. *Proc. Natl Acad. Sci. USA*, **96**, 6171–6176.
54. Torres,T. and Levitus,M. (2007) Measuring conformational dynamics: a new FCS-FRET approach. *J. Phys. Chem. B*, **111**, 7392–400.
55. Lee,J.Y., Okumus,B., Kim,D.S. and Ha,T. (2005) Extreme conformational diversity in human telomeric DNA. *Proc. Natl Acad. Sci. USA*, **102**, 18938–18943.
56. Santalucia,J. Jr. (1998) A unified view of polymer, dumbbell, and oligonucleotide DNA nearest-neighbor thermodynamics. *Proc. Natl Acad. Sci. USA*, **95**, 1460–1465.
57. Peyret,N., Seneviratne,P.A., Allawi,H.T. and Santalucia,J Jr (1999) Nearest-neighbor thermodynamics and nmr of dna sequences with internal A·A, C·C, G·G, and T·T mismatches. *Biochemistry*, **38**, 3468–3477.
58. Phan,A.T. and Patel,D.J. (2003) Two-repeat human telomeric d(TAGGGTTAGGGT) sequence forms interconverting parallel and antiparallel G-quadruplexes in solution: distinct topologies, thermodynamic properties, and folding/unfolding kinetics. *J. Am. Chem. Soc.*, **125**, 15021–15027.